J Nanopart Res (2016) 18:92
DOI 10.1007/s11051-016-3400-7

RESEARCH PAPER

Bio-inactivation of human malignant cells through highly responsive diluted colloidal suspension of functionalized magnetic iron oxide nanoparticles

Roberta V. Ferreira · Priscila P. Silva-Caldeira · Elene C. Pereira-Maia · José D. Fabris · Luis Carlos D. Cavalcante · José D. Ardisson · Rosana Z. Domingues

Received: 24 November 2015 / Accepted: 19 March 2016 / Published online: 30 March 2016

Abstract Magnetic fluids, more specifically aqueous colloidal suspensions containing certain magnetic nanoparticles (MNPs), have recently been gaining special interest due to their potential use in clinical treatments of cancerous formations in mammalians. The technological application arises mainly from their hyperthermic behavior, which means that the nanoparticles dissipate heat upon being exposed to an alternating magnetic field (AMF). If the temperature is raised to slightly above 43 °C, cancer cells are functionally inactivated or killed; however, normal cells tend to survive under those same conditions, entirely maintaining their bioactivity. Recent in vitro studies have revealed that under simultaneous exposure to an AMF and magnetic nanoparticles, certain lines of cancer cells are bio-inactivated even without experiencing a significant temperature increase. This non-thermal effect is cell specific, indicating that MNPs, under alternating magnetic fields, may effectively kill cancer cells under conditions that were previously thought to be implausible, considering that the temperature does not increase more than 5 °C, which is also true in cases for which the concentration of MNPs is too low. To experimentally test for this effect, this study focused on the feasibility of inducing K562 cell death using an AMF and aqueous suspensions containing very low concentrations of MNPs. The assay was designed for a ferrofluid containing magnetite nanoparticles, which were obtained through the co-precipitation method and were functionalized with citric acid; the particles had an average diameter of 10 ± 2 nm and a mean hydrodynamic diameter of

R. V. Ferreira
Department of Materials, Federal Center of Technological Education of Minas Gerais, Nova Suíça, Belo Horizonte 30421-169, Brazil

P. P. Silva-Caldeira
Department of Chemistry, Federal Center of Technological Education of Minas Gerais, Nova Suíça, Belo Horizonte 30421-169, Brazil

E. C. Pereira-Maia · J. D. Fabris · L. C. D. Cavalcante · R. Z. Domingues (✉)
Department of Chemistry – ICEx, Federal University of Minas Gerais (UFMG), Belo Horizonte, MG 31270-901, Brazil
e-mail: rosanazd@yahoo.com.br; rosanazd@ufmg.br

J. D. Fabris
Federal University of the Jequitinhonha and Mucuri Valleys (UFVJM), PRPPG, Campus JK, Diamantina, MG 39100-00, Brazil

L. C. D. Cavalcante
Center of Natural Sciences, Federal University of Piauí (UFPI), Teresina, PI 64049-550, Brazil

J. D. Ardisson
Nuclear Technology Development Center (CDTN), Belo Horizonte, MG 31270-901, Brazil

approximately 40 nm. Experiments were first performed to test for the ability of the ferrofluid to release heat under an AMF. The results show that for concentrations ranging from 2.5 to 1.0×10^3 mg L^{-1}, the maximum temperature increase was actually less than 2 °C. However, the in vitro test results from K562 cells and suspensions containing these MNPs at concentrations varying within a narrower range from 2.5 to 10 mg L^{-1}, typically under an AMF of 15 kA m^{-1} at 356 kHz, indicate efficient cytotoxic activity against malignant cells and inhibition of cell growth, even at very low hyperthermally induced temperature increases. The IC_{50} value varied with time, reaching 3.5 mg L^{-1} after 10 min under the AMF. Our results effectively demonstrate new prospective uses for such nanoparticles in advanced medical practices in oncology.

Keywords Magnetite nanoparticles · Nanotechnology · Chemical functionalization · Magnetic hyperthermia · Cancer therapy · Nanomedicine

Introduction

Magnetic hyperthermia is a cancer therapy based on alternating magnetic fields (AMFs) and magnetic nanoparticles acting as heat-dissipating agents. In this therapy practice, magnetic nanoparticles resonantly respond to an alternating magnetic field by converting the magnetic energy into heat; this capability is due to superparamagnetism. This hyperthermic effect can be used in the treatment of cancer by exposing tumorous organs or tissues to locally controlled higher temperatures (42–46 °C), which tend to damage and kill malignant cells (Ito et al. 2005; Mahmoudi et al. 2011; Laurent et al. 2011; Salunkhe et al. 2014). In 2010, the treatment of tumors using magnetite nanoparticles as agents to generate intra-tissue heat received the approval of the European Regulatory Agency as a new clinical therapy (MagForce 2010).

Most significantly, these studies have demonstrated cancer cell death only if the temperature is raised above 43 °C by the heat dissipation of magnetic nanoparticles following AMF exposure (4.5). However, it has been recently reported that magnetic nanoparticles in AMFs were able to induce dramatic cell death without increasing the temperature of the bulk solution (Creixell et al. 2011; Villanueva et al. 2010; Asín et al. 2012). The non-thermal effect is cell type specific, indicating that in alternating magnetic fields, MNPs may effectively kill cancer cells under conditions previously considered implausible, i.e., temperature increases less than 5 °C, low concentrations of MNPs, and low magnetic field amplitudes and frequencies. Recent studies have reported that only WEHI-164 (Jadhav et al. 2013), MDA-MB-468 and MCF-7 (Creixell et al. 2011), He-La (Villanueva et al. 2010), MDA-MB (Thomas et al. 2011), and dendritic cells (Marcos-Campos et al. 2011; Asín et al. 2013) showed significant cell death after AMF and magnetic nanoparticle exposure without a temperature increase (Goya et al. 2013).

Nanoparticles of magnetic iron oxides, such as magnetite and maghemite, are particularly attractive for biomedical and biotechnological applications as they exhibit superparamagnetic behavior with suitable saturation magnetization, as well as relatively high magnetic susceptibilities and biocompatibility (Gamarra et al. 2010; Hergt and Andra 2007; Ho et al. 2011; Jordan et al. 1999; Kulshrestha et al. 2012; Laurent et al. 2008; Neuberger et al. 2005; Sharifi et al. 2012; Tartaj et al. 2003). Magnetite and maghemite are materials that are broadly tested as hyperthermia agents in different sizes and shapes and that can be injected either intratumorally or intravenously. However, these materials tend to self-aggregate and form large agglomerates due to their anisotropic dipolar attraction. These agglomerates make nanoparticle suspensions structurally unstable, leading to the loss of critical properties related to the magnetic monodomain structures, such as the superparamagnetism. The nanosized dimensions also increase the chemical reactivity of these particles, resulting in much faster degradation in biological environments (Pankhurst et al. 2003; Ito et al. 2005; Laurent et al. 2011). This lack of stability tends to restrict the application of magnetite nanoparticles in clinical practices. Conversely, the colloidal stability can be significantly improved through surface functionalization (Mout et al. 2012; Hosseini et al. 2013; Deng et al. 2014) with peptides (Cavalli et al. 2012; Wei et al. 2013), nucleic acids (Nyamjav and Ivanisevic 2005) (DNA, RNA), silica (Ferreira et al. 2010a, b), polymers (Lee et al. 2004; Gupta and Gupta 2005; Reddy et al. 2007; Hajdú et al. 2012), or small molecules, such as carboxylates and phosphates (Ferreira et al. 2010a;

Sousa et al. 2013; Saraswathy et al. 2014). The colloidal stability of suspensions in biological environments under a magnetic field is a very important feature for biomedical and biotechnological applications. Functional agents prevent the formation of large agglomerates in aqueous environments, thereby providing the technological alternative of obtaining stable colloidal suspensions (Berry and Curtis 2003; Harris et al. 2003; Illés and Tombácz 2006; Faraji and Wipf 2009; Ding et al. 2010; Frimpong et al. 2010; Huang and Juang 2011; Hajdú et al. 2012; Nguyen 2013; Saraswathy et al. 2014).

This report describes a detailed study on the feasibility of inactivating K562 human tumor cells via a method involving the increase of the local temperature surrounding the cells by exposing functionalized MNPs to an AMF. To so do, magnetite nanoparticles were first synthesized, and MNP crystallographic and hyperfine structures, chemical composition, morphology, size, and thermogravimetric behavior were analyzed. The magnetite nanoparticles were then functionalized with citric acid in an attempt to obtain stable suspensions that could be suitably and safely used as cancer therapy agents. Temperature dependence on the AMF and nanoparticle concentration in the aqueous ferrofluid was first assessed in an attempt to determine the optimal conditions for obtaining only slight or moderate local temperature increases.

Experimental details

Materials

Ferrous chloride ($FeCl_2{\cdot}4H_2O$), ferric chloride ($FeCl_3{\cdot}6H_2O$), hydrochloric acid (HCl), citric acid, and ammonium hydroxide (NH_4OH) were purchased from Sigma-Aldrich, USA. All chemicals were analytical grade with 99.99 % purity and were used without further purification.

Synthesis of the magnetite nanoparticles

The synthesis of the magnetite nanoparticles was performed using the co-precipitation method. The synthesis consisted of mixing $FeCl_3{\cdot}6H_2O$ and $FeCl_2{\cdot}4H_2O$ at a stoichiometric ratio of 2:1 (Fe^{3+}/Fe^{2+}) in an alkaline medium (Ferreira et al. 2010a, b). The material was lyophilized; this sample was labeled "Mag."

Citric acid magnetite nanoparticle surface modification

The chemical functionalization was conducted by adding citric acid to the suspension containing the magnetite nanoparticles (Mag) in water. The suspension was stirred for 30 min at 80 °C. The sample was washed with water to remove the excess citric acid, and the sample was then lyophilized (Ferreira et al. 2010a); this sample was labeled "MagCA."

Suspensions were prepared with the MagCA material at concentrations of 1.0, 2.0, and 10.0 g L^{-1} in water at near-neutral pH (7.0–7.4), and the suspensions were sonicated for 6 h.

Physicochemical characterization

The X-ray diffraction patterns were obtained using a Geigerflex model Rigaku diffractometer, with Co(Kα) radiation, over a range from 20° to 80° (2θ) at a rate of 4° per minute; standard silicon was used as an external standard. The XRD data were numerically refined through the least-squares method using the FullProf fitting program (version January 2011).

Fourier transform infrared (FTIR) spectra were obtained through transmission mode in a Perkin-Elmer Spectrum GX spectrometer. The samples were ground, dispersed in KBr, and pressed into tablets. The spectra were obtained over the interval of 4000–400 cm^{-1} with a resolution of 4 cm^{-1}.

Thermogravimetric analyses were performed in a Netzsch STA 409EP thermobalance under N_2 flux. An initial mass of ~10 mg was heated from 30 to 750 °C at a rate of 10 °C/min with a gas flow of 100 mL min^{-1}.

Quantification of the iron oxide in the MagCA sample was performed by the colorimetric method with ortho-phenanthroline. The absorbance of the solutions was obtained at 510 nm in a spectrophotometer UV–Visible Shimadzu UV-mini, according to a method reported by Schwertmann and Cornell (2003).

The mean hydrodynamic diameter and polydispersity index (PDI) of the iron oxide nanoparticle suspensions were determined using dynamic light scattering (Nano Size ZS equipment). Intensity correlation functions were measured at a scattering angle of $\theta = 90°$ using a wavelength of 633 nm. All reported hydrodynamic diameters were calculated using the

Stokes–Einstein equation, $r_h = kT/(6\pi\eta D)$, where k is Boltzmann's constant, T is the temperature, η is the solvent viscosity, D is the diffusion constant, and r_h is the hydrodynamic radius of the spherical particle. The zeta potential of the iron oxide nanoparticle suspensions was evaluated by the electrophoretic mobility of charged particles using phase analysis light scattering and Nano Size ZS equipment. For the measurements, the MagCA and Mag samples were dispersed in water and sonicated for 6 h. The pH of these solutions was measured and adjusted with either aqueous KOH 10^{-3} mol L^{-1} or HNO_3 10^{-3} mol L^{-1}; the particle sizes were measured as a function of pH.

The samples were imaged using transmission electron microscopy (TEM); a Tecnai G2-20—SuperTwin FEI microscope was used with an accelerating voltage of 200 kV. Several drops of the nanoparticle suspensions were deposited on microscope grids; the images were captured once the solvent had evaporated.

The Mössbauer spectra were collected in constant acceleration transmission mode with a ~15 mCi Co^{57}/Rh gamma-ray source. A spectrometer equipped with a transducer (CMTE model MA250) controlled by a linear function driving unit (CMTE model MR351) was used to obtain the spectra at 298 and 150 K. The Mössbauer isomer shifts shown are relative to an α-Fe foil at room temperature. The experimental data were least-squares fitted to Lorentzian functions using NORMOS^{TM}–90 software.

Heating ability studies

Heat dissipation measurements were accomplished using Easy Heat Ambrell equipment. MagCA aqueous suspension aliquots (2 mL) of different concentrations (0.0025–10 g L^{-1}) were placed inside plastic tubes and positioned in the middle of an induction coil operating at a frequency of 356 kHz. AMF with an amplitude of 15 kA m^{-1} was applied initially for 30 s. The temperature increase was measured after exposure to the AMF with a TEPSE digital thermometer model WT-1. The procedure was repeated after increasing the exposure time in the intervals of 30 s. The SAR values were calculated according to Eq. (1):

$$\mathrm{SAR} = \frac{\sum_i C_i m_i}{m}\frac{\Delta T}{\Delta t}, \quad (1)$$

where $C_i m_i$ is the heat capacity of the component i, in which the temperature is to be increased by applying the AMF, m is the mass of the magnetic iron oxide component, and $\frac{\Delta T}{\Delta t}$ is the initial slope of the temperature (T)−time (t) dependence profile, which is defined as being the first 60 s ($t = 0$) immediately after the magnetic field is applied. The calculations were based on the specific heat capacity of water, 4.18 J g^{-1} K^{-1}; the product $C_i m_i$ is insignificant for magnetite nanoparticles compared with the quantity $C_i m_i$ for water.

Cell culture

The K562 cell line originated from the pleural effusion of a 53-year-old woman who developed chronic myelogenous leukemia and was in terminal blast crisis; K562 cells were purchased from the Rio de Janeiro Cell Bank (index at the RJCB collection # CR083). The cells were cultured in RPMI 1640 (Sigma) medium supplemented with 10 % fetal calf serum (Cultlab; São Paulo, Brazil) at 37 °C in a humidified atmosphere with 5 vol% CO_2. The cells grew exponentially from 1×10^5 to approximately 8×10^5 cells mL^{-1} over 3 days. Cell viability was assessed using the trypan blue exclusion protocol. The number of cells was determined according to Coulter counter analysis.

Cell growth inhibition

For the cytotoxicity assessment, 1×10^5 cells mL^{-1} were cultured for 48 h with different concentrations of MagCA. Control experiments were conducted according to the same protocol described but without nanoparticles. Cell sensitivity to the nanoparticles was evaluated by the concentration required to inhibit 50 % of cellular growth, otherwise known as the IC_{50} index. The concentrations used in the cytotoxicity assays ranged from 0 to 0.01 g L^{-1}. Cell viability was again assessed using the trypan blue exclusion protocol.

Cell growth inhibition with magnetic field exposure

For the cytotoxicity studies under a magnetic field, approximately 10^5 cells were suspended in 1 mL of

the culture medium (RPMI 1640 with 10 % of fetal serum). With different concentrations of nanoparticles, which ranged from 0 to 0.004 g L^{-1}, the cells were submitted to a magnetic field of 15 kA m^{-1} at 356 kHz for 5 or 10 min. The cells were then incubated for 48 h; the IC_{50} value was determined as described above. To determine whether exposure to the magnetic field affected cell viability, control experiments were conducted following this same protocol but without nanoparticles. All of the assays were conducted in triplicate.

Results and discussion

Physicochemical characterization

The powder X-ray diffraction (XRD) patterns for the Mag sample are presented in Fig. 1. The main characteristic peaks were obtained with the (h k l) values of (2 2 0), (3 1 1), (4 0 0), (4 2 2), and (5 1 1). From the Rietveld refinement ($\chi^2 = 2.12$), the observed value, $a = 8.396$ Å, is the standard value reported on the JCPDS card # 19-629. This strongly indicates that magnetite was the only or the major crystalline phase in this Mag sample (Roca et al. 2007). The mean coherent length, which reflects the mean particle size of the Mag sample, was found to be 9 nm, as calculated using the Scherrer formula.

The FTIR spectrum collected over the range from 450 to 4000 cm^{-1} for the MagCA sample (Fig. 2a) shows a band at 590 cm^{-1} corresponding to the

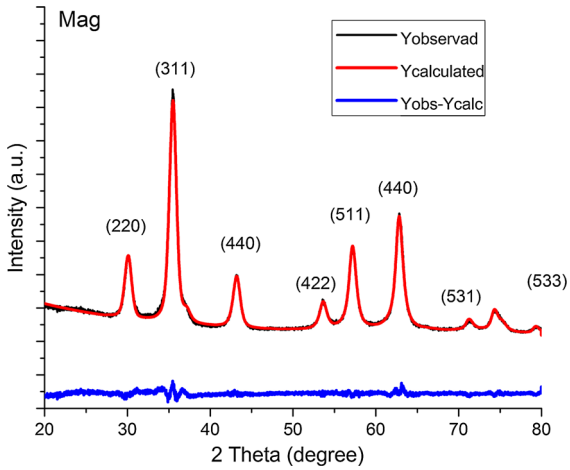

Fig. 1 Rietveld refinement pattern for the Mag sample

symmetric stretch of the Fe–O bond. The intense band at 3414 cm^{-1} can be assigned to the stretching of hydroxyl groups that include contributions from the –OH group of water molecules, which are thought to adsorb onto the surface of the iron oxide particles; carboxylic acid group stretching also contributes to this band. The band at 2924 cm^{-1} is related to the stretching of the $–CH_2$ group. The citric acid bound onto the surface of the magnetite nanoparticles may be responsible for the shifted bands at 1617 and 1387 cm^{-1}. These shifts are related to the symmetric and asymmetric stretches of the C–O group of the citric acid molecules, which are characteristically centered at 1633 and 1376 cm^{-1}, respectively (Harris et al. 2003; Zhang et al. 2006; Roca et al. 2007).

The thermal weight loss curve (TG; Fig. 2b) shows three stages, and the differential thermal analysis curve (DTA) consistently shows three exothermal events. The first mass loss (4 %), which occurs in the range of 31–108 °C, is related to the loss of water adsorbed on the surface of the magnetite nanoparticles. The second (19 %) and third (6 %) stages can be interpreted as being due to the decomposition of citric acid adsorbed on the surface of the magnetite nanoparticles, which are shown as exothermal peaks at 207 and 398 °C. These latter events corresponded to 25 % of the mass reduction, which indicated that the chemical functionalization yielded magnetite nanoparticles that were 25 % w/w citric acid. The chemical quantification of the iron oxide component of the sample, conducted using the ortho-phenanthroline method (Stucki 1981), indicated that the citric acid content corresponded to approximately 20 mass%, which was very similar to the value obtained by TGA.

The TEM images (Fig. 3) allowed inferences about the shape, size, and uniformity of the particles before and after being chemically functionalized. In effect, the magnetite nanoparticles were found to be almost spherical and highly agglomerated, with a narrow size distribution and a mean diameter of 10 ± 2 nm, as shown in Fig. 3a, b. This result is very close to 9 nm, which was the mean coherent length value obtained from the XRD data using the Scherrer formula.

Functionalizing the magnetite nanoparticles with citrate groups lowered the mean particle size to a mean diameter of $d = 7 \pm 2$ nm and narrowed the size distribution (insets of Fig. 3a, b).

The TEM images (Fig. 3a, b) show that the Mag sample was composed of agglomerates with a mean

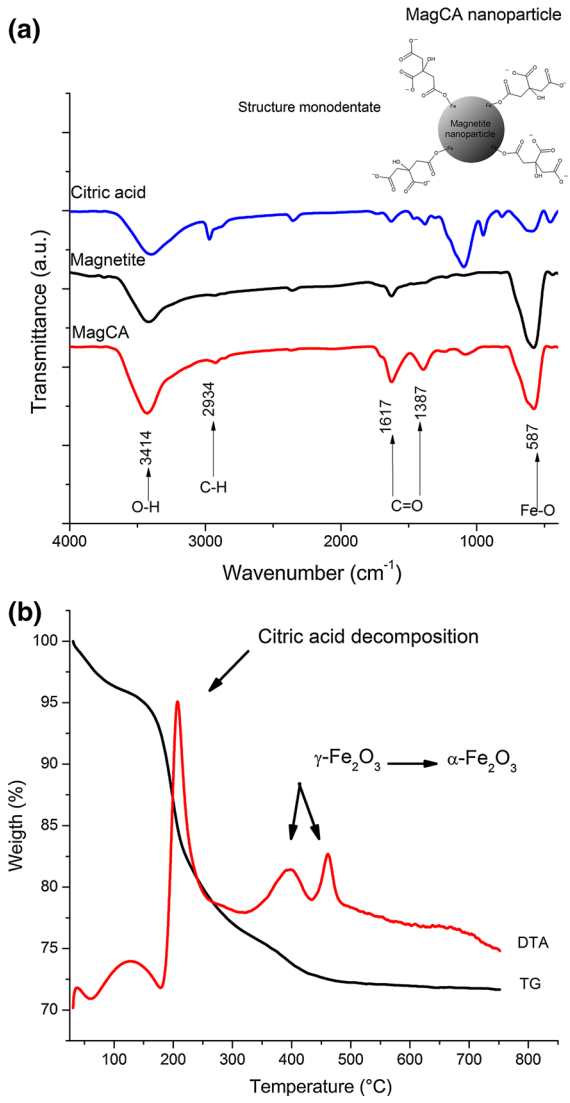

Fig. 2 FTIR spectra of **a** MagCA, Mag, and citric acid and **b** TG–DTA curves for MagCA

diameter of approximately 50 nm, which decreased upon coating the nanoparticles. The MagCA sample exhibited a lower degree of agglomeration than that of the Mag sample. This is likely because of the presence of the citric acid layer on the magnetite surface (Sousa et al. 2013; Saraswathy et al. 2014). The average hydrodynamic diameter (D_h = 238 nm) and the polydispersity index PDI (0.419) obtained for the Mag sample through dynamic light scattering (DLS) measurements also suggest that this suspension sample was composed of agglomerated particles. The PDI indicates a heterogeneous population in relation to size. The zeta potential of the Mag suspension sample at a pH of 7 was low (−9.8 mV), which is characteristic of an unstable suspension with agglomerated particles.

DLS analysis of the MagCA suspension showed that the average hydrodynamic diameter was 85 nm, and the polydispersity index was 0.17. In comparison with the DLS results of the non-functionalized sample, these results indicate that the size distribution became more homogeneous after the nanoparticles were coated with citric acid. The zeta potential was also a much higher value (−39.7 mV) that was typical for a stable suspension (ZetaSizer Nano Series User Manual 2004).

Stability

To evaluate the stability of the magnetite nanoparticles as a function of time, ^{57}Fe Mössbauer measurements were performed using samples that had been aged for approximately 1 month (Fig. 4).

The experimental Mössbauer spectrum for the Mag sample was least-squares fitted with two blocks of model-independent hyperfine field distribution (Fig. 5); one block was for the A sites (Fe^{3+}–O in tetrahedral coordination sites), and the other block was for the B sites (electronically coupled Fe^{3+}–O and Fe^{2+}–O in octahedral sites) of the magnetite structure. The resonance lines in all cases were asymmetrically broadened in comparison with the typical symmetrical Lorentzian shape, as would be expected for pure bulk magnetite. Following this fitting model, the isomer shift values were made to linearly vary with the hyperfine field values. The probability profiles of the hyperfine field distribution for the month-old Mag samples were nearly similar to those measured at the time of synthesis. The same was true for the hyperfine field and isomer shift values. Regarding the values of the Mössbauer parameters for all measurements (Table 1), the hyperfine fields at maximum probability, B_{hf}^{max}, were found at 45(1) and 46(1) T, with the corresponding averaged isomer shifts relative to αFe, $\bar{\delta}/\alpha Fe$ = 0.27(4) and 0.27(3) mm s^{-1}, respectively, for the tetrahedral sites; B_{hf}^{max} = 41.7(4) and 43.7(8) T and $\bar{\delta}/\alpha Fe$ = 0.73(1) and 0.58(2) mm s^{-1}, respectively, were found for the octahedral sites. These data, together with those from XRD and FTIR, confirm the occurrence of magnetite in the Mag sample.

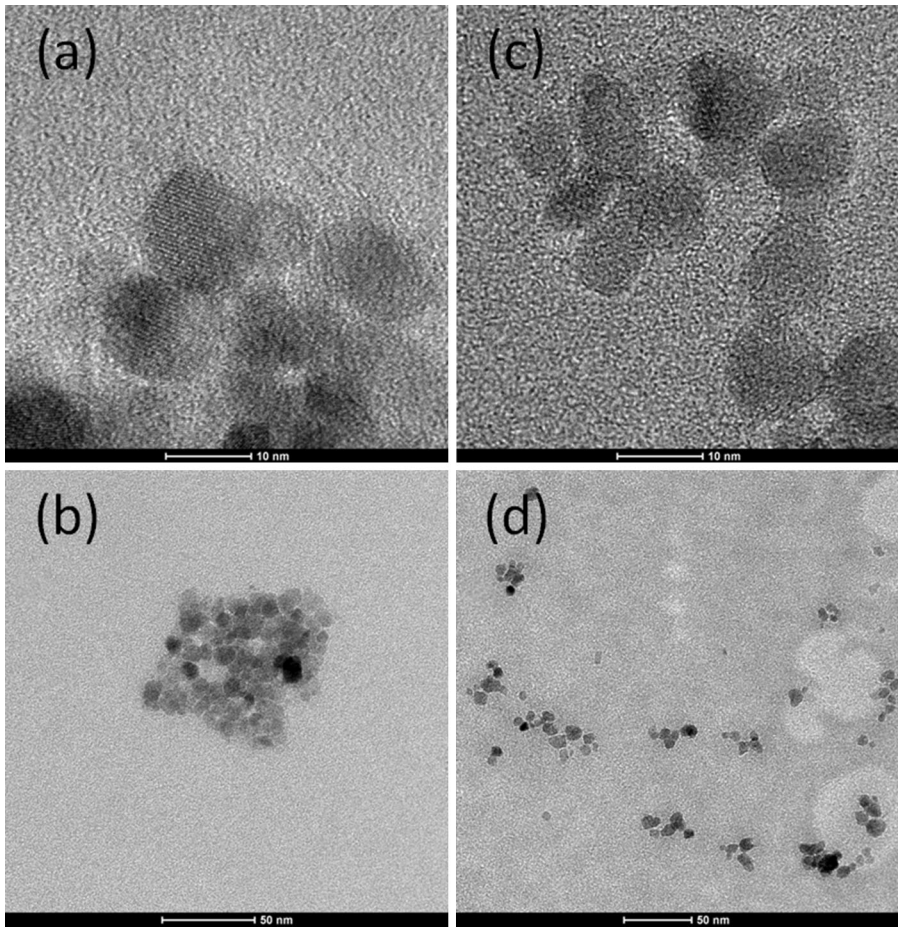

Fig. 3 TEM images of the **a** Mag and **b** MagCA samples. *Inset* shows particle size and size distribution for Mag and MagCA samples

The differences between the spectra obtained for this magnetite sample and the typical spectra expected for bulk magnetite can be due to several reasons. According to data reported in the literature (Morup et al. 1976; Roca et al. 2007), the small particle size distribution may lead to an inhomogeneous hyperfine coupling and asymmetric line broadening. Magnetic relaxation effects in a suspension of small particles with a given size distribution may cause line broadening and asymmetry of the resonance lines, relative to the theoretical Lorentzian shape (Morup et al. 1976).

No substantial difference was observed in the Mössbauer spectra and their corresponding set of hyperfine parameters between the measurements obtained from Mag samples at the time of synthesis and those obtained a month after synthesis, which indicates that this synthetic iron oxide is chemically stable on a reasonable time scale.

Mag and MagCA samples were independently synthesized and prepared the same way as the previous preparations were with the specific purpose of assessing any eventual chemical effects of the citric acid layer on the hyperfine structure of the iron oxide. Any such effect would sensitively be reflected by differences in chemical, crystallographic, or magnetic structure. The Mössbauer spectra taken from samples at 150 K, well above the Verwey transition temperature of $T_V \sim 120$ K, are presented in Fig. 6. The numerical analysis performed by fitting these experimental spectra with an independent hyperfine field distribution led to the probability profiles shown in Fig. 7. From these results, the two expected sites (Table 2) for magnetite were still identified through the mixed valence $Fe^{3+/2+}$ in octahedral sites, for which the averaged isomer shift ($\bar{\delta}/\alpha$Fe) value relative to the αFe was relatively higher than that of Fe^{3+}

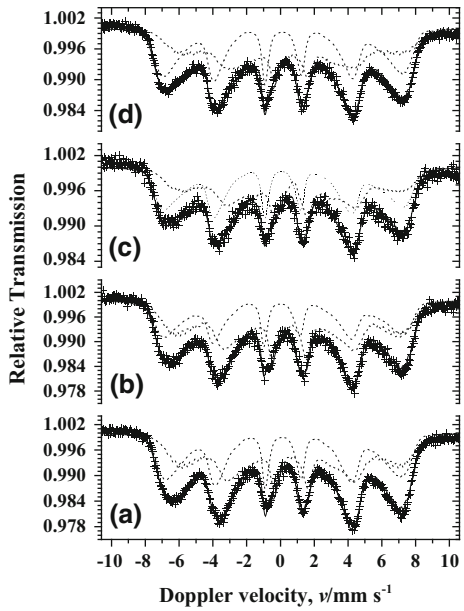

Fig. 4 Mössbauer spectra at 298 K for the Mag sample. Stability of the magnetite nanoparticles as a function of time: **a** at the time of synthesis and **b** 11 days, **c** 17 days, and **d** 30 days after synthesis

(relatively lower $\bar{\delta}/\alpha$Fe values) in tetrahedral Fe–O polyhedra. These data show that the partial sum of the subspectral areas due to the assigned mixed valence octahedral $Fe^{3+/2+}$ of the Mag sample (RA = 54.6 %) corresponds well to that of the MagCA sample (RA = 58.6 %). The sum of the corresponding subspectral areas of Fe^{3+} in tetrahedral sites (RA = 45.4 % for Mag and RA = 41.4 % for MagCA) must complement the whole individual spectrum of magnetite, as no other iron-bearing species was assigned for either of these two samples. The hyperfine field values (Table 2) were also comparable for the corresponding octahedral sites [Mag sample, B_{hf}^{max} = 37(2), 43(2), 47(1), and 50.2(8) T; MagCA sample, B_{hf}^{max} = 37(4), 44(4), 47(1), and 50.0(8) T] and tetrahedral sites [Mag sample, B_{hf}^{max} = 35.5(5), 43(2), 48(1), and 50.6(9) T; MagCA sample, B_{hf}^{max} = 36.6(3), 44(4), 48(2), and 50.2(6) T] for the two samples. Each of these maximum hyperfine field values at 150 K most likely corresponds to a hyperfine interaction of a given fraction of the particle size distribution in the sample. If that is true, further cooling the samples might block any remaining magnetic relaxation to yield spectra with narrower resonance lines.

The differences in the relative individual areas (Table 2), in which the partial area due to each fraction of iron sites was numerically decomposed in Gaussian profiles, are due to numerical uncertainties in fitting the probability curves. Therefore, the hypothesis of the influence of the citric acid layer on the hyperfine structure of the as-prepared iron oxide is negligible; no effect of the citric acid layer on the iron oxide structure could be clearly observed.

Figure 8a presents zeta potential as a function of pH for these magnetite nanoparticles, before and after citric acid functionalization. The isoelectronic points of the functionalized and non-functionalized samples were found to be pH = 3.0 and 6.9, respectively. This shift corroborates the surface modification of the particles in the sample after being coated with citric acid.

Figure 8b shows the zeta potential and hydrodynamic diameter of this magnetite as functions of pH. The zeta potential observed at pH values below 3.0 was considered to be rather low, meaning that the particles surfaces are not electrically charged to a large extent. The dipolar attraction between the magnetic dipoles of the nanoparticles causes the particles to agglomerate. This explains the large average hydrodynamic diameters (1770 and 1860 nm) in comparison with the size of the nanoparticles (10 nm). In the pH range from 4.0 to 6.0, most of the citrate groups are chemically dissociated, and this creates negative charges on the surface of the coated magnetite nanoparticles. Although the suspension is still composed of agglomerated particles between pH 4.0 and 6.0, the zeta potential increases by 18–24 mV, meaning that the hydrodynamic diameter is much smaller, such as 456, 286, and 204 nm. Above pH 7.0, all the acid groups are deprotonated, causing the surface charge to be even more negative. When zeta potential reached more negative values that are typical of a stable suspension, specifically, −39 mV, the average hydrodynamic diameter was reduced to 85 nm. This value tended to remain the same at pH 8.0 and 9.0, indicating that in this range, the particle surface was sufficiently charged, resulting in an electrical repulsion among the particles. The observed variation of the hydrodynamic diameter as a function of pH was thus consistently in agreement with the zeta potential values.

To evaluate the stability of the suspensions as a function of time, the hydrodynamic diameters were

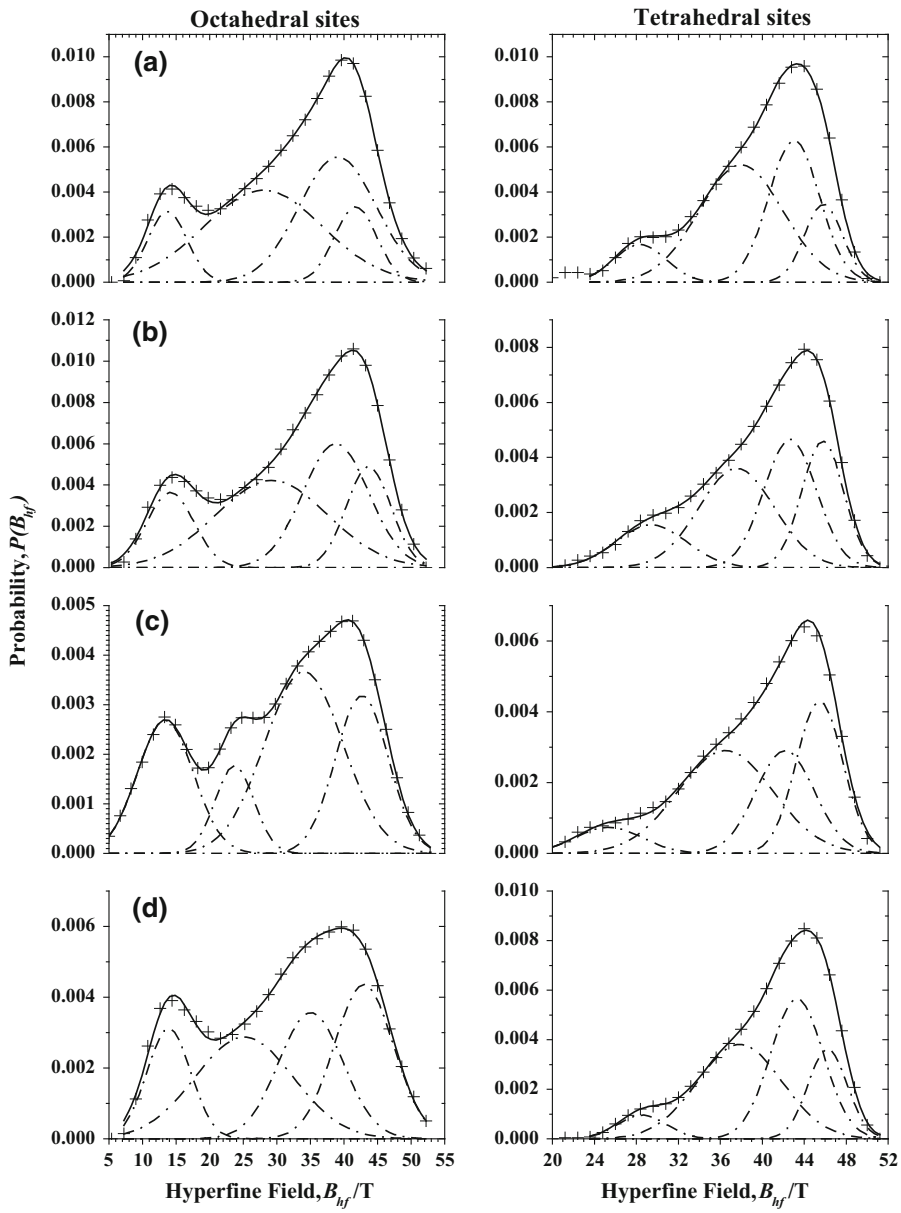

Fig. 5 Hyperfine field distribution of the tetrahedral sites and the octahedral sites. **a** At the time of synthesis and **b** 11 days, **c** 17 days, and **d** 30 days after synthesis

continuously measured over a period of 7 days. Figure 9a shows that the MagCA sample did not present any significant variation in hydrodynamic diameter during the 7 days. During the same period, the Mag sample presented an increase of approximately 100 % of the initial hydrodynamic diameter value. Comparing these results with those obtained for the non-functionalized magnetite nanoparticles, the pH 7.0 aqueous suspension of functionalized particles was significantly different.

Suspension stability was also monitored by UV–Vis absorbance for 7 days (Fig. 9b). In the first 5 h, measurements were carried out at intervals of 1 h (inset Fig. 9b). Other measurements were performed after 24, 48, and 72 h as well as 7 days. In the first 5 h, the stability of the suspension of the functionalized magnetite nanoparticles (MagCA) was noticeably higher than that of the non-functionalized particles (Mag). After 1 h, the absorbance of the Mag sample had significantly dropped, whereas the absorbance of

Table 1 298 K-Mössbauer parameters for the Mag sample deduced from model-independent hyperfine field distributions

Measurement	Assignment	$\bar{\delta}/\alpha$Fe	B_{hf}^{max}	RA (%)
Readily after the synthesis	$Fe^{3+/2+}$	0.71(1)	13.7(2)	5.79(1)
		0.72(1)	28(7)	22.76(8)
		0.73(1)	39(2)	20.25(7)
		0.73(1)	41.7(4)	6.66(1)
	Fe^{3+}	0.20(2)	28.3(6)	3.96(1)
		0.26(2)	38(4)	20.00(1)
		0.28(2)	43(3)	14.6(1)
		0.31(2)	46(1)	5.98(1)
11 days after the synthesis	$Fe^{3+/2+}$	0.60(2)	14.2(2)	8.40(1)
		0.59(2)	29(9)	23.1(1)
		0.59(2)	39(7)	19.3(2)
		0.58(2)	43.7(8)	10.8(1)
	Fe^{3+}	0.12(3)	29(3)	5.15(1)
		0.19(3)	38(5)	12.80(7)
		0.23(3)	43(2)	11.4(1)
		0.27(3)	46(1)	9.05(5)
17 days after the synthesis	$Fe^{3+/2+}$	0.85(3)	13.39(9)	11.64(1)
		0.79(3)	23.7(2)	5.31(1)
		0.73(3)	34(1)	22.30(2)
		0.69(3)	42.7(6)	13.06(2)
	Fe^{3+}	0.15(4)	25(2)	3.37(1)
		0.22(4)	37(7)	18.91(6)
		0.25(4)	42(7)	11.7(1)
		0.27(4)	45(1)	13.71(6)
30 days after the synthesis	$Fe^{3+/2+}$	0.70(1)	13.9(3)	8.16(1)
		0.72(1)	25(8)	16.80(7)
		0.74(1)	35(4)	13.68(1)
		0.75(1)	43(3)	15.45(1)
	Fe^{3+}	0.17(2)	28.5(7)	2.65(1)
		0.23(2)	38(4)	18.29(4)
		0.25(2)	43(2)	16.94(7)
		0.28(2)	46.2(9)	8.03(1)

Stability of the magnetite nanoparticles as a function of time. $Fe^{3+/2+}$ = mixed valence iron in octahedral sites; Fe^{3+} iron in tetrahedral sites; $\bar{\delta}/\alpha$Fe = averaged isomer shift relative to αFe; B_{hf}^{max} = maximum-probability hyperfine field and RA = relative subspectral area

the MagCA sample remained constant. The MagCA absorbance behavior indicates that the functionalization improved the stability of the suspension, at least for the first 5 h. Even after 7 days, the observed decrease in absorbance was only marginally significant.

Heating capability studies

To evaluate the heating dissipation profile of the MagCA suspension, an in vitro study was carried out using an AMF frequency of 356 kHz and a field strength of 15 kA m^{-1}. Figure 10 presents the time dependence of the temperature for the aqueous suspensions containing MagCA nanoparticles, which varied in concentration from 0.0025 to 10 g L^{-1}.

As clearly shown in Fig. 10, the rate of temperature increase is strongly concentration dependent. The more concentrated is the suspension, the higher is the temperature increase. The results also show that for the magnetic nanoparticle concentrations ranging from 0.0025 to 1.0 g L^{-1}, the temperature increase was not enough to reach 43 °C. It was possible to reach hyperthermic temperatures, i.e., an increase of

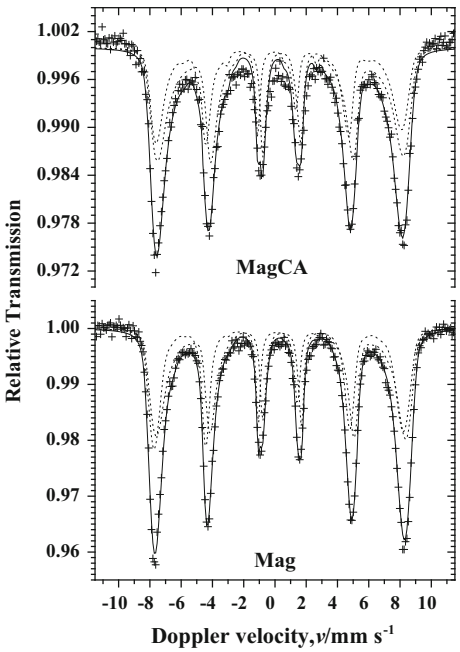

Fig. 6 Mössbauer spectra at 150 K for the Mag and MagCA samples

the medium temperature of approximately 5 °C, only with magnetite nanoparticle suspension concentrations up to 2.0 g L^{-1}.

The SAR coefficient revealed that the heat production efficiency decreased with the MagCA concentration. The SAR values obtained from MagCA suspension concentrations of 1.0, 2.0, and 10.0 g L^{-1} were 139, 70, and 14 W g^{-1}, respectively. The highest SAR value (139 W g^{-1}) was obtained from the suspension with the lowest concentration (1.0 g L^{-1}); these results show that the SAR value decreases with increasing concentrations of particles in suspension. This behavior is related to the relaxation mechanism of heat dissipation. The magnitude of the heating scale is strongly influenced by interparticle interactions. If the magnetite nanoparticle concentration increases in the suspension, the first consequence is that the mean distance between adjacent magnetic particles is reduced. If the system is further exposed to an external AMF, the magnetic dipolar interaction will become relevant, and the interactions among the particles will inhibit the relaxation mechanism, resulting in lower SAR values.

Effect of MagCA on cellular growth with or without magnetic field exposure

The viability tests were based on assays involving the exposure of ferrofluids with very low concentrations of nanoparticles to the AMF. The results shown above

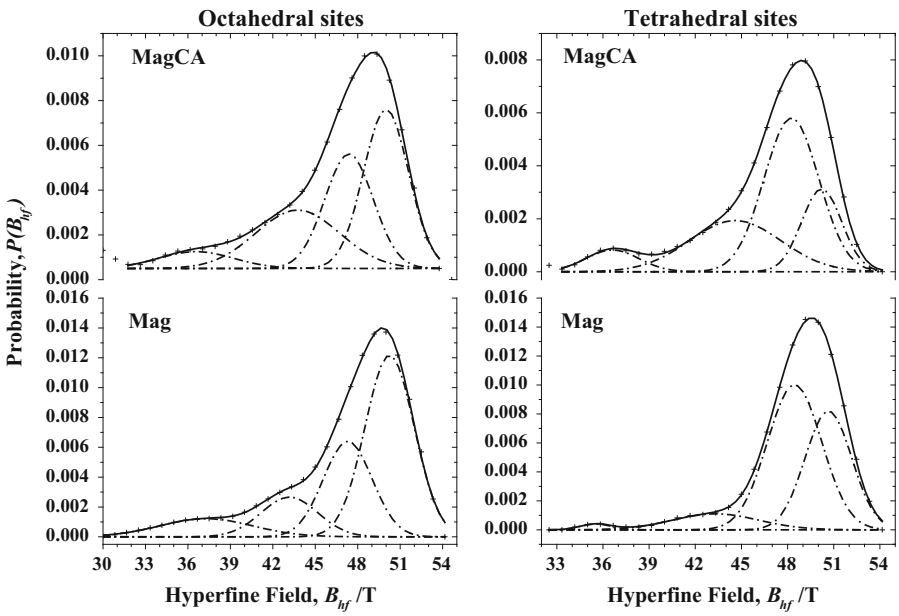

Fig. 7 Hyperfine field distribution for the tetrahedral sites and the octahedral sites

Table 2 150 K-Mössbauer parameters for the Mag and MagCA samples deduced from model-independent hyperfine field distributions

Sample	Assignment	$\bar{\delta}/\alpha$Fe	B_{hf}^{max}	RA (%)
Mag	$Fe^{3+/2+}$	0.56(3)	37(2)	5.26(1)
		0.54(3)	43(2)	7.03(2)
		0.53(3)	47(1)	27.80(3)
		0.52(3)	50.2(8)	14.52(4)
	Fe^{3+}	0.07(3)	35.5(5)	0.54(1)
		0.21(3)	43(2)	4.18(1)
		0.29(3)	48(1)	23.89(5)
		0.34(3)	50.6(9)	16.78(4)
MagCA	$Fe^{3+/2+}$	0.44(3)	37(4)	3.90(1)
		0.47(3)	44(4)	15.20(4)
		0.49(3)	47(1)	17.23(4)
		0.50(3)	50.0(8)	22.31(2)
	Fe^{3+}	0.08(3)	36.6(3)	2.72(1)
		0.22(3)	44(4)	11.02(2)
		0.28(3)	48(2)	19.83(4)
		0.32(3)	50.2(6)	7.79(3)

$Fe^{3+/2+}$ = mixed valence iron in octahedral sites; Fe^{3+} iron in tetrahedral sites; $\bar{\delta}/\alpha$Fe = averaged isomer shift relative to αFe; B_{hf}^{max} = maximum-probability hyperfine field; and RA = relative subspectral area

demonstrate that exposing MagCA suspensions with nanoparticle concentrations from 0.0025 to 1.0 g L^{-1} to the AMF leads to a maximum temperature increase of approximately 2 °C, which is not sufficient to cause direct hyperthermic effects. This concentration range was thus chosen for the K562 cell viability tests.

After choosing the optimal magnetite nanoparticle concentration range for the suspension, the first cell viability assay was conducted with the higher concentration (1 g L^{-1}) in the absence of an AMF. Regarding cell viability, this concentration was found to be too high; it was not possible to observe the cell growth because the particles tended to cover the cells. Thus, cell viability was evaluated using diluted suspensions ranging from 0.0002 to 0.0100 g L^{-1}. The viability tests were performed both with and without an alternating magnetic field within this concentration range.

Figure 11a shows the viability of K562 cells that were exposed to different suspension concentrations of the MagCA sample. Predictably, for the tested concentration range, cell viability was not significantly affected by the suspensions without the application of an AMF. Even at the highest concentration tested, 0.0100 g L^{-1}, cell viability was still above 80 % (Fig. 11a). These results were very different when the cells were exposed to a magnetic field for 5 min (15 kA m^{-1} and 356 kHz). The cytotoxic effect of MagCA became greatly enhanced, and this was reflected by an IC_{50} = 0.0025 g L^{-1} (Fig. 11b). A further increase of the exposure time to 10 min led to an increase of cytotoxicity and an IC_{50} = 0.00035 - g L^{-1}. No effect of the magnetic field application on

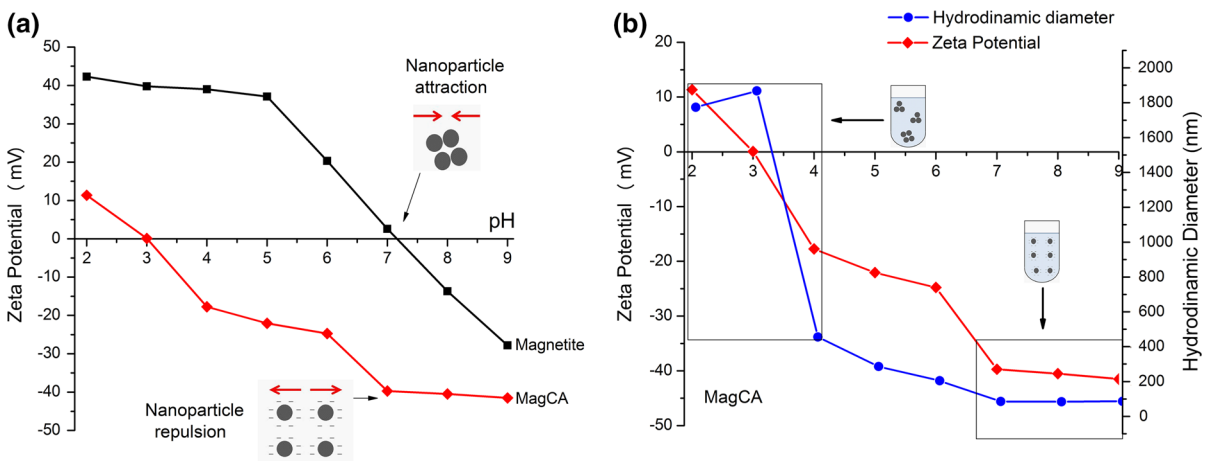

Fig. 8 **a** Zeta potential measurements as a function of pH for the MagCA and Mag samples and **b** zeta potential and hydrodynamic diameter measurements for the MagCA sample

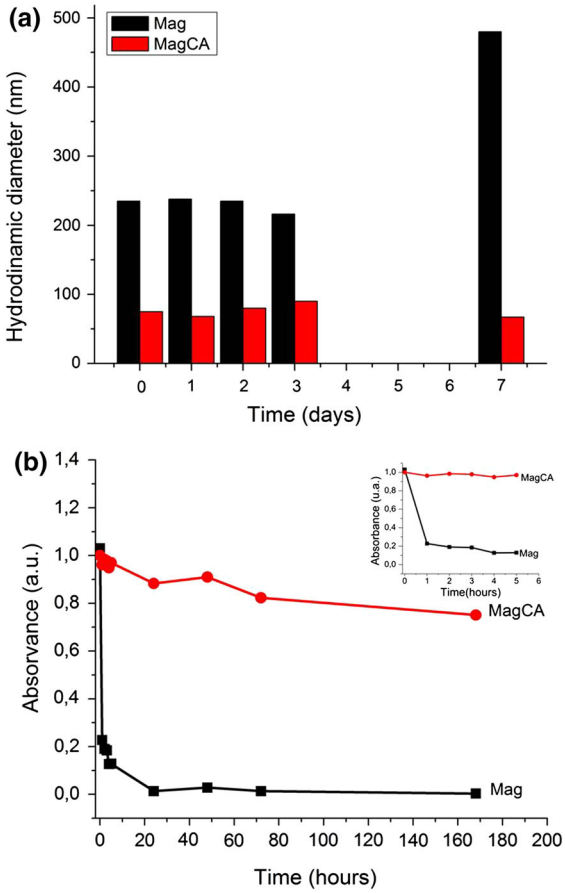

Fig. 9 **a** Hydrodynamic diameter measurements as a function of time and **b** UV–Vis absorbance measurements as a function of time for the Mag and MagCA samples

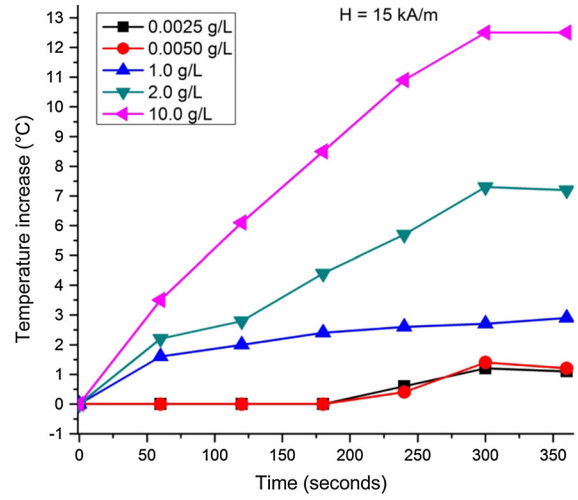

Fig. 10 **a** Temperature versus time of exposure to a 15 kA m^{-1} AMF for MagCA aqueous suspensions of different concentrations

cellular viability (15 kA m^{-1} and 356 kHz for 5 min) was observed in the absence of the nanoparticles.

These results are very promising, and particularly a hyperthermia effect (i.e., no significant temperature increase) was not directly invoked and cannot explain the cytotoxic effect. From the data shown in Fig. 11b, one can see that a 5-min application of the magnetic field on a stable aqueous suspension of MagCA in the concentration range from 0.0025 to 0.005 g L^{-1} increases the medium temperature by only 1 °C. Therefore, our results indicate that an AMF exposure induces a significant cytotoxic effect against tumor

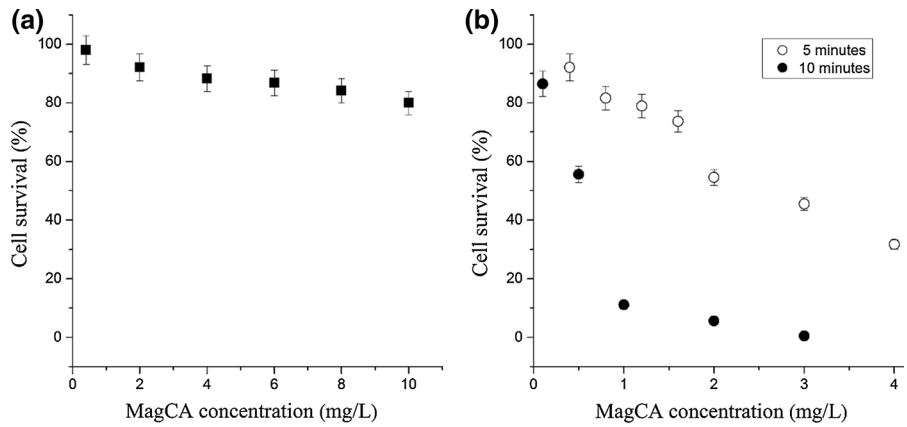

Fig. 11 **a** Effect of MagCA concentration on cell growth without an AMF. The values are the mean of triplicate determinations. **b** Effect of MagCA concentration on cell growth with an AMF. The cells were exposed to a magnetic field (15 kA m^{-1} and 356 kHz) for 5 min (*open circles*) and for 10 min (*filled circles*). The values are the mean of triplicate determinations (Morup et al. 1976)

cells without requiring a significant increase in temperature. The mechanism of the induction of the cytotoxic action by AMF application remains to be clarified. However, it is clear that under the experimental conditions of these assays, hyperthermia alone cannot be responsible for the increased cytotoxicity observed in the K562 cells.

These findings are substantially relevant, as they indicate that no local high-temperature side effects, which are often associated with this type of oncological therapy, would now harm the treated human tissue. In addition, hyperthermic heating also would be a particularly restrictive technique for addressing the treatment of small tumors or metastatic cancers, which usually require high concentrations of magnetite nanoparticles to increase the temperature sufficiently (Hergt and Dutz 2007). Our results show that relatively low concentrations of MagCA can inhibit tumor cell growth with very low temperature changes relative to that of a normal, living human body. The considerable inhibitory effect of the MagCA nanoparticles on cell growth under the application of a magnetic field opens a new window for the technological development of cancer therapy.

Conclusions

In this work, magnetite nanoparticles were easily prepared through the co-precipitation method. The obtained X-ray diffraction results indicated that the magnetite nanoparticles only exhibited the spinel phase of Fe_3O_4. The Mössbauer measurements revealed that the magnetite nanoparticles appeared to be chemically stable over time. No substantial differences in hyperfine parameters were observed for the synthetic iron oxide. The size of the particles determined using transmission electronic microscopy and DLS showed that the sample was composed of isolated particles 10 nm in diameter that formed large, heterogeneous agglomerates. The polydispersity index showed that in an aqueous suspension, the magnetite nanoparticles exhibited a large size distribution. Characterization of the magnetite nanoparticle suspension performed using UV–Visible spectrophotometry, dynamic light scattering, and zeta potential measurements indicated that at a pH close to 7, the aqueous magnetite nanoparticle suspension was not stable, which explains the need for surface functionalization.

The surface functionalization of the Fe_2O_3 nanoparticles was successfully achieved using citric acid molecules. FTIR spectroscopy, thermal analysis, and zeta potential measurements confirmed this modification. The size of the particles after functionalization was 7 nm, and the large agglomerates were dispersed. This effect is beneficial and demonstrates the efficacy of this method. The aqueous MagCA suspension showed relatively higher stability compared with that of the non-functionalized sample at a pH close to 7.0. Even after 7 days, the functionalized formulation remained stable with no increase in particle size or agglomerate formation.

The studies on temperature increase in the presence of an AMF showed that the nanoparticle concentration had an effect on the efficiency of the dissipation of heat. The assays examining the relation between temperature and nanoparticle concentration under an AMF indicated that the magnetic nanoparticle concentrations did not exhibit local macroscopic temperature increases. The functionalized magnetite nanoparticles alone did not affect the growth of tumor (i.e., chronic myelogenous leukemia) cells; however, under the application of a magnetic field, a considerable inhibition of growth was observed. The in vitro tests showed significant cytotoxic effects even at very low nanoparticle concentrations. The temperature was found to be nearly constant, suggesting that the K562 cells did not experience any direct thermal effects that would cause cytotoxicity. The substantial inhibitory effect on cell growth exerted by very low concentrations of the stable MNP suspensions under the application of a magnetic field opens a new possibility for the use of magnetite nanoparticles in cancer therapy without requiring a significant temperature increase.

Acknowledgments This work was supported by the Minas Gerais State Agency for the Development of Scientific Research (FAPEMIG; Brazil), the National Institute of Science and Technology for Catalysis (INCT-Catálise; Brazil), and the National Council for Scientific and Technological Development (CNPq; Brazil). JDF would like to thank the Coordination of Superior Level Staff Improvement (CAPES; Brazil) for granting his Visiting Professorship at the Federal University of the Jequitinhonha and Mucuri Valleys (UFVJM; Brazil) under the PVNS program and the CNPq for Grant # 305755-2013-7. LCDC is currently a postdoctoral fellow at UFMG.

References

Andrade AL, Ferreira RV, Fabris JD, Domingues RZ (2011) Coating nanomagnetic particles for biomedical applications. In: Fazel R (ed) Biomedical engineering: frontiers and challenges. Nova Publishers, New York, pp 379–392. ISBN 978-953-307-309-5

Asín L, Ibarra MR, Tres S, Goya GF (2012) Controlled cell death by magnetic hyperthermia: effects of exposure time, field amplitude, and nanoparticle concentration. Pharm Res 29:1319–1327. doi:10.1007/s11095-012-0710-z

Asín L, Goya GF, Tres A, Ibarra MR (2013) Induced cell toxicity originates dendritic cell death following magnetic hyperthermia treatment. Cell Death Dis 4:e596. doi:10.1038/cddis.2013.121

Berry CC, Curtis ASG (2003) Functionalisation of magnetic nanoparticles for applications in biomedicine. J Phys D Appl Phys 36:R198–R206

Cavalli S, Carbajo D, Acosta M, Lope-Piedrafita S, Candiota AP, Arús C, Royo M, Albericio F (2012) Efficient γ-amino-proline-derived cell penetrating peptide–superparamagnetic iron oxide nanoparticle conjugates via aniline-catalyzed oxime chemistry as bimodal imaging nanoagents. Chem Commun 48:5322–5324. doi:10.1039/c2cc17937g

Creixell M, Bohorquez AC, Torres-Lugo M, Rinaldi C (2011) EGFR-targeted magnetic nanoparticle heaters kill cancer cells without a perceptible temperature rise. ACS Nano 5:7124–7129. doi:10.1021/nn201822b

Deng M, Huang Z, Zou Y, Yin G, Liu J, Gu J (2014) Fabrication and neuron cytocompatibility of iron oxide nanoparticles coated with silk-fibroin peptides. Coll Surf B 116:465–471. doi:10.1016/j.colsurfb.2014.01.021

Ding J, Tao K, Li J, Song S, Sun K (2010) Cell-specific cytotoxicity of dextran-stabilized magnetite nanoparticles. Coll Surf B 79:184–190. doi:10.1016/j.colsurfb.2010.03.053

Faraji AH, Wipf P (2009) Nanoparticles in cellular drug delivery. Bioorg Med Chem 17:2950–2962. doi:10.1016/j.bmc.2009.02.043

Ferreira RV, Pereira ILS, Cavalcante LCD, Gamarra LF, Carneiro SM, AmaroJr E, Fabris JD, Domingues RZ, Andrade AL (2010a) Synthesis and characterization of silica-coated nanoparticles of magnetite. Hyperfine Interact 195:265–274. doi:10.1007/s10751-009-0128-0

Ferreira RV, Fabris JD, Domingues RZ (2010b) Preparation of biocompatible ferrofluids for magnetic hyperthermia studies. Nanotechnol Res J 3:289–302

Frimpong RA, Dou JD, Pechan M, Hilt JZ (2010) Enhancing remote controlled heating characteristics in hydrophilic magnetite nanoparticles via facile co-precipitation. J Magn Magn Mater 322:326–331. doi:10.1016/j.jmmm.2009.09.050

Gamarra LF, Mamani JB, Carneiro SM, Fabris JD, Ferreira RV, Domingues RZ, Cornejo DR, Pontuschka WM, Amaro E (2010) Characterization of superparamagnetic iron oxide coated with silicone used as contrast agent for magnetic resonance image for the gastrointestinal tract. J Nanosci Nanotechnol 10:1153–1158. doi:10.1166/jnn.2010.1843

Goya GF, Lima E Jr, Arelaro AD, Torres T, Rechenberg HR, Rossi L, Marquina C, Ibarra MR (2008) Magnetic hyperthermia with Fe_3O_4 nanoparticles: The influence of particle size on energy absorption. IEEE Trans Magn 44:4444–4447. doi:10.1109/TMAG.2008.2003508

Gupta AK, Gupta M (2005) Synthesis and surface engineering of iron oxide nanoparticles for biomedical applications. Biomaterials 26:3995–4021. doi:10.1016/j.biomaterials.2004.10.012

Hajdú A, Szekeres M, Tóth IY, Bauer RA, Mihály J, Zupkó I, Tombácz E (2012) Enhanced stability of polyacrylate-coated magnetite nanoparticles in biorelevant media. Coll Surf B 94:242–249. doi:10.1016/j.colsurfb.2012.01.042

Harris L, Goff J, Carmichael A, Riffle J, Harburn J, Pierre TGS, Saunders M (2003) Magnetite nanoparticle dispersions stabilized with triblock copolymers. Chem Mater 15:1367–1377. doi:10.1021/cm020994n

Hergt R, Andra W (2007) Magnetic hyperthermia and thermoablation. In: Andra W, Nowak H (eds) Magnetism in medicine. A Handbook. WILEY-VCH, Weinheim, pp 550–567

Hergt R, Dutz S (2007) Magnetic particle hyperthermia-biophysical limitations of a visionary tumour therapy. J Magn Magn Mater 311:187–192. doi:10.1016/j.jmmm.2006.10.1156

Ho J, Al-Deen FM, Al-Abboodi A, Selomulya C, Xiang SD, Plebanski M, Forde GM (2011) N,N-Carbonyldiimidazole-mediated functionalization of superparamagnetic nanoparticles as vaccine carrier. Coll Surf B 83:83–90. doi:10.1016/j.colsurfb.2010.11.001

Hosseini F, Panahifar A, Adeli M, Amiri H, Lascialfari A, Orsini F, Doschak MR, Mahmoudi M (2013) Synthesis of pseudopolyrotaxanes-coated superparamagnetic iron oxide nanoparticles as new MRI contrast agent. Coll Surf B 103:652–657. doi:10.1016/j.colsurfb.2012.10.035

Huang SH, Juang RS (2011) Biochemical and biomedical applications of multifunctional magnetic nanoparticles: a review. J Nanopart Res 13:4411–4430. doi:10.1007/s11051-011-0551-4

Illés E, Tombácz E (2006) The effect of humic acid adsorption on pH-dependent surface charging and aggregation of magnetite nanoparticles. J Coll Int Sci 295:115–123. doi:10.1016/j.jcis.2005.08.003

Ito A, Shinkai M, Honda H, Kobayashi T (2005) Medical application of functionalized magnetic nanoparticles. J Biosci Bioeng 100:1–11. doi:10.1263/jbb.100.1

Jadhav NV, Prasad AI, Kumar A, Mishra R, Dhara S, Babu KR, Prajapat NL, Ningthoujam RS, Pandey BN, Vatsa RK (2013) Synthesis of oleic acid functionalized Fe_3O_4 magnetic nanoparticles and studying their interaction with tumor cells for potential hyperthermia applications. Colloid Surf B Biointerfaces 108:158–168. doi:10.1016/j.colsurfb.2013.02.035

Jordan A, Scholz R, Wust P, Schirra H, Schiestel T, Schmidt H, Felix R (1999) Endocytosis of dextran and silan-coated magnetite nanoparticles and the effect of intracellular hyperthermia on human mammary carcinoma cells in vitro. J Magn Magn Mater 194:185–196. doi:10.1016/S0304-8853(98)00558-7

Kulshrestha P, Gogoia M, Bahadur D, Banerjee R (2012) In vitro application of paclitaxel loaded magnetoliposomes for combined chemotherapy and hyperthermia. Coll Surf B 96:1–7. doi:10.1016/j.colsurfb.2012.02.029

Laurent S, Forge D, Port M, Roch A, Robic C, Vander Elst L, Muller RN (2008) Magnetic iron oxide nanoparticles: synthesis, stabilization, vectorization, physicochemical characterizations, and biological applications. Chem Rev 108:2064–2110. doi:10.1021/cr068445e

Laurent S, Dutz S, Häfeli UO (2011) Magnetic fluid hyperthermia: focus on superparamagnetic iron oxide nanoparticles. Adv Coll Interface Sci 166:8–23. doi:10.1016/j.cis.2011.04.003

Lee SJ, Jeong JR, Shin SC, Kim JC, Chang YH et al (2004) Nanoparticles of magnetic ferric oxides encapsulated with poly(D, L lactide-co-glycolide) and their applications to magnetic resonance imaging contrast agent. J Magn Magn Mater 272–276:2432–2433. doi:10.1016/j.jmmm.2003.12.416

MagForce AG (2010). http://www.magforce.de/en/unternehmen/ueber-uns.html. Accessed 6 Oct 2015

Mahmoudi M, Sant S, Wang F, Laurent S, Sen T (2011) Superparamagnetic iron oxide nanoparticles (SPIONs): development, surface modification and applications in chemotherapy. Adv Drug Deliv Rev 63:24–46. doi:10.1016/j.addr.2010.05.006

Marcos-Campos I, Asin L, Torres TE, Marquina C, Tres A, Ibarra MR, Goya GF (2011) Cell death induced by the application of alternating magnetic fields to nanoparticle-loaded dendritic cells. Nanotechnology 22:1–9. doi:10.1088/0957-4484/22/20/205101

Morup S, Topsoe E, Lipka L (1976) Modified theory for Mössbauer spectra of superparamagnetic particles: application to Fe_3O_4. J Phys Colloq 37:C6-287–C6-290. doi:10.1051/jphyscol:1976658

Mout R, Moyano DF, Rana S, Rotello VM (2012) Surface functionalization of nanoparticles for nanomedicine. Chem Soc Rev 41:2539–2544. doi:10.1039/C2CS15294K

Neuberger T, Schöpf B, Hofmann H, Hofmann M, Von Rechenberg B (2005) Superparamagnetic nanoparticles for biomedical applications: possibilities and limitations of a new drug delivery system. J Magn Magn Mater 293:483–496. doi:10.1016/j.jmmm.2005.01.064

Nguyen TD (2013) Portraits of colloidal hybrid nanostructures: controlled synthesis and potential applications. Coll Surf B 103:326–344. doi:10.1016/j.colsurfb.2012.10.049

Nyamjav D, Ivanisevic A (2005) Templates for DNA-templated Fe_3O_4 nanoparticles. Biomaterials 26:2749–2757. doi:10.1016/j.biomaterials.2004.07.025

Pankhurst QA, Connolly J, Jones SK, Dobson J (2003) Applications of magnetic nanoparticles in biomedicine. J Phys D 36:167

Reddy KR, Lee KP, Iyengar AG (2007) Synthesis and characterization of novel conducting composites of Fe_3O_4 nanoparticles and sulfonated polyanilines. J Appl Polym Sci 104:4127–4134. doi:10.1002/app.26020

Roca AG, Marco JF, del Puerto Morales M, Serna CJ (2007) Effect of nature and particle size on properties of uniform magnetite and maghemite nanoparticles. J Phys Chem C 111:18577–18584. doi:10.1021/jp075133m

Salunkhe AS, Khot VM, Pawar SH (2014) Magnetic hyperthermia with magnetic nanoparticles: a status review. Curr Top Med Chem 14:572–594. doi:10.2174/1568026614666140118203550

Saraswathy A, Nazeer SS, Jeevan M, Nimi N, Vijayakumar S, Harikrishnanc S, Harikrishna PR, Ramapurath V, Jayasreea S (2014) Citrate coated iron oxide nanoparticles with enhanced relaxivity for in vivo magnetic resonance imaging of liver fibrosis. Coll Surf B 117:216–224. doi:10.1016/j.colsurfb.2014.02.034

Schwertmann U, Cornell RM (2003) The iron oxides: structure, properties, occurrences and uses. WILEY-VCH, Weinheim

Sharifi I, Shokrollahi H, Amiri S (2012) Ferrite-based magnetic nanofluids used in hyperthermia applications. J Magn Magn Mater 324:903–915. doi:10.1016/j.jmmm.2011.10.017

Sousa ME, van Raap MBF, Rivas PC, Zélis PM, Girardin P, Pasquevich GA, Alessandrini JL, Muraca D, Sánchez FH (2013) Stability and relaxation mechanisms of citric acid coated magnetite nanoparticles for magnetic hyperthermia. J Phys Chem C 117:5436–5445. doi:10.1021/jp311556b

Stucki JW (1981) The quantitative assay of minerals for Fe^{2+} and Fe^{3+} using 1,10-phenanthroline. II. A photochemical method. Soil Sci Soc Am J 45:638–641

Tartaj P, Morales MP, Veintemillas-Verdaguer S, González-Carreno T, Serna CJ (2003) The preparation of magnetic nanoparticles for applications in biomedicine. J Phys D 36:R182–R197. doi:10.2136/sssaj1981

Thomas OC, Hedayati M, Zhou H, Zheng Y, Wabler M, Mihalic J, Geyh A, Ivkov R, Deweese TL (2011) Thermal and non-thermal effects of membrane bound ferromagnetic nanoparticles. Int J Radiat Oncol Biol Phys 81:S749–S750. doi:10.1016/j.ijrobp.2011.06.1242

Villanueva A, Presa P, Alonso JM, Rueda T, Martínez A, Crespo P, Morales MP, Gonzalez-Fernandez MA, Valdés J, Rivero G (2010) Hyperthermia HeLa cell treatment with silica-coated manganese oxide nanoparticles. J Phys Chem C 114:1976–1981. doi:10.1021/jp907046f

Wei Y, Yin G, Ma C, Huang Z, Chen X, Liao X, Yao Y, Yin H (2013) Synthesis and cellular compatibility of biomineralized Fe_3O_4 nanoparticles in tumor cells targeting peptides. Coll Surf B 107:180–188. doi:10.1016/j.colsurfb.2013.01.058

ZetaSizer Nano Series User Manual (2004) Malvern Instruments Ltd., Malvern, Worcestershire

Zhang L, He R, Gu HC (2006) Oleic acid coating on the monodisperse magnetite nanoparticles. Appl Surf Sci 253:2611–2617. doi:10.1016/j.apsusc.2006.05.023